



## Ion Beam Radiation Effects in Monazite.

Valérie Picot, Xavier Deschanel, Sylvain Peugot, Benoit Glorieux,  
Anne-Magali Seydoux-Guillaume, Richard Wirth

► **To cite this version:**

Valérie Picot, Xavier Deschanel, Sylvain Peugot, Benoit Glorieux, Anne-Magali Seydoux-Guillaume, et al.. Ion Beam Radiation Effects in Monazite.. Journal of Nuclear Materials, Elsevier, 2008, 381 (3), pp.290-296. <10.1016/j.jnucmat.2008.09.001>. <hal-00606691>

**HAL Id: hal-00606691**

**<https://hal.archives-ouvertes.fr/hal-00606691>**

Submitted on 7 Jul 2011

**HAL** is a multi-disciplinary open access archive for the deposit and dissemination of scientific research documents, whether they are published or not. The documents may come from teaching and research institutions in France or abroad, or from public or private research centers.

L'archive ouverte pluridisciplinaire **HAL**, est destinée au dépôt et à la diffusion de documents scientifiques de niveau recherche, publiés ou non, émanant des établissements d'enseignement et de recherche français ou étrangers, des laboratoires publics ou privés.

## Ion Beam Radiation Effects in Monazite

V. Picot<sup>1</sup>, X. Deschanel<sup>2</sup>, S. Peugeot<sup>2</sup>, B. Glorieux<sup>3</sup>, A.M. Seydoux-Guillaume<sup>4</sup>, R. Wirth<sup>5</sup>

<sup>1</sup>*Centre d'Études et de Recherches par Irradiation, UPR 33, 45071 Orléans Cedex 2, France*

<sup>2</sup>*Institut de Chimie Séparative de Marcoule, CEA Valrhô Marcoule,  
UMR 5257, BP 17171, 30207 Bagnols-sur Cèze, France*

<sup>3</sup>*Laboratoire des Procédés, Matériaux et Énergie Solaire, UPR 8521,  
Rambla de la Thermodynamique, 66100 Perpignan, France*

<sup>4</sup>*Laboratoire des Mécanismes et Transferts en Géologie, UMR 5563 UR 14,  
Observatoire Midi-Pyrénées, 14 avenue Édouard Belin, 31400 Toulouse, France*

<sup>5</sup>*GeoForschungsZentrum Potsdam, PB 4.1, Telegrafenberg, 14473 Potsdam, Germany*

### Abstract

Monazite is a potential matrix for conditioning minor actinides arising from spent fuel reprocessing. The matrix behavior under irradiation must be investigated to ensure long-term containment performance. Monazite compounds were irradiated by gold and helium ions to simulate the consequences of alpha decay. This article describes the effects of such irradiation on the structural and macroscopic properties (density, hardness) of monazites  $\text{LaPO}_4$  and  $\text{La}_{0.73}\text{Ce}_{0.27}\text{PO}_4$ . Irradiation by gold ions results in major changes in the material properties. At a damage level of 6.7 dpa, monazite exhibits volume expansion of about 8.1%, a 59% drop in hardness, and structure amorphization, although Raman spectroscopy analysis shows that the phosphate-oxygen bond is unaffected. Conversely, no change in the properties of these compounds was observed after He ion implantation. These results indicate that ballistic effects predominate in the studied dose range.

**Keywords:** Monazite, Irradiation effects, Hardness, Density, XRD, Raman spectroscopy; Deposited energy

**PACS:** 81.05.Je, 61.82-d, 61.80.Jh, 28.41.Kw

**Corresponding author:**

Tel: +33-4 66 79 60 87, Fax: +33-4 66 79 76 11, e-mail: xavier.deschanel@cea.fr

## 1. Introduction

Monazite compounds have been a subject of particular interest since the 1980s as a potential matrix for conditioning the minor actinides [1]. Monazite is a rare earth orthophosphate  $\text{Ln}^{3+}\text{PO}_4$  (where “Ln” is La to Gd) crystallizing in a monoclinic system (space group  $\text{P}2_1/n$ ,  $Z = 4$ ). It consists of alternating chains of  $\text{PO}_4$  tetrahedra and  $\text{LnO}_9$  polyhedra. Tetravalent cations can be incorporated with a divalent cation at the lanthanide site. In this case the orthophosphate  $\text{Ca}^{2+}\text{B}^{4+}(\text{PO}_4)_2$  is called brabantite by mineralogists, although its crystallographic structure is exactly the same as that of monazite. The solid solution between the pure monazite  $\text{Ln}^{3+}\text{PO}_4$  and brabantite  $\text{Ca}^{2+}\text{B}^{4+}(\text{PO}_4)_2$  allows simultaneous loading of trivalent and tetravalent cations.

Most studies of natural analogs concern ceramics incorporating trivalent lanthanides and tetravalent actinides such as uranium and thorium. These natural monazite-brabantite solid solutions are capable of incorporating actinides in large quantities (up to 15 oxide wt% thorium and 6 oxide wt% of uranium) [2-4]; they exhibit good chemical durability [5] and are never metamict despite sometimes very high integrated doses ( $\sim 2 \times 10^{20}$   $\alpha/\text{g}$ , i.e. 14 dpa) [6-8], indicating a structure with satisfactory self-irradiation resistance. Experimental studies show that monazite is able to restore its structure at low temperature [9].

The literature includes many publications on synthetic compounds doped with trivalent [10-16] or tetravalent [17-19] actinides, but relatively few papers dealing with compounds incorporating both tri- and tetravalent elements [20]. These studies describe structural modifications (amorphization) and microstructural changes (swelling) in the materials as a result of cumulative irradiation damage arising from alpha decay. Amorphization of  $^{238}\text{PuPO}_4$  was observed at a dose of  $8.6 \times 10^{17}$   $\alpha/\text{g}$  (0.1 dpa), whereas  $(\text{La}, ^{238}\text{Pu})\text{PO}_4$  remained crystallized after integrated doses of up to  $2.5 \times 10^{18}$   $\alpha/\text{g}$  (0.25 dpa) [21]. Moreover, in addition to the amorphization process, a crystal lattice volume increase of about 1.1% was observed in  $^{241}\text{AmPO}_4$  ceramics after integrating a dose of  $8.3 \times 10^{17}$   $\alpha/\text{g}$  (0.1 dpa) [22].

External irradiation has also been used to simulate alpha decay, and shows that monazite can be amorphized by heavy ions (Kr) for damage of less than 2 dpa [23-24]. However, the monazite structure can be easily be restored by annealing at low-temperature (300°C) [25] or under an electron beam [24-26].

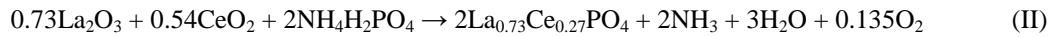
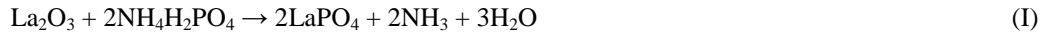
The self-irradiation behavior of monazite combines two opposing phenomena: defect creation by alpha disintegration, and low-temperature annealing capacity for the recrystallization of the structure. This dichotomy is no doubt responsible for the very scattered critical amorphization doses (0.1 to 2 dpa) reported for this structure in the literature [21-23].

In this work we have attempted to elucidate the underlying mechanisms responsible for the long-term changes in the properties of the monazite matrix. We used external irradiation to simulate the consequences of cumulative alpha decay on the structure and properties of monazite. The use of different elements (Au, He) to irradiate the samples allowed us to discriminate between damage caused by the recoil nucleus and by the recoil nucleus and by the alpha particle.

## 2. Experimental

### 2.1. Sample preparation

Two rare earth orthophosphates,  $\text{LaPO}_4$  and  $\text{La}_{0.73}\text{Ce}_{0.27}\text{PO}_4$ , were prepared by solid-phase reaction according to the protocol described by Montel [27]. This synthesis route involves the following reactions:



The specific surface area was increased by attrition milling of the precursors and calcined powder samples in a zirconia jar for 2 h at 450 rpm with zirconia beads 1 and 2 mm in diameter (50% of each size), then oven-dried at 100°C.

Pellets were produced by 70 MPa uniaxial press compaction at room temperature, then sintered in air for 4 hours at 1450°C. The geometric density of the sintered pellets was determined by weighing and dimensional measurements (Table 1).

#### Insert Table 1

XRD analysis confirmed that the crystallized and monoclinic structure of both compounds studied. No secondary phase was detected using this technique. The measured lattice parameters were consistent with published data (Table 1) [19, 28]. Scanning electron microscope examination (Fig. 1 and 2) confirmed that both materials were single-phase compounds.

#### Insert Figure 1 – Figure 2

### 2.2. Ion beam irradiation

The integrated dose variation versus time after disposal in a monazite-brabantite compound incorporating 10 oxide wt% actinide oxides is shown in Fig 3.

#### Insert Figure 3

Alpha decay generates a recoil nucleus with an energy between 70 and 100 keV and a very high-energy alpha particle of about 5 MeV that captures two electrons to produce a helium atom in the structure. The kinetic energy of these particles is deposited in the host material by two distinct processes [30]:

- ballistic processes corresponding to elastic collisions between atomic nuclei, resulting in atomic displacements; the energy deposited by this process is written  $E_{nuct}$ .
- ionization and electronic excitation processes resulting in a temperature rise in the material and capable under certain conditions of inducing a few atomic displacements; the energy deposited by this process is written  $E_{elec}$ .

The energy fractions transferred by the two process for external irradiation and actinide-doped materials are indicated in Table 2. The recoil nucleus has a range of about 40 nm in the material and transfers its energy mainly through ballistic processes, causing many atomic displacements ( $\approx 1500$  displacements per event). The alpha particle has a range of a few tens of micrometers, transferring virtually all its energy through process ionization and, near the end of its track, a very small fraction in the form of elastic collisions generating about 100 atomic displacements.

#### **Insert Table 2**

To a large extent external irradiation with He and Au ions can be used to simulate energy deposits corresponding respectively to the alpha particle and recoil nucleus. In the case of irradiation by helium ions the energy fractions ( $f_{elec}$  and  $f_{nuct}$ ) are practically identical to those of the decay alpha particle, whereas with Au ions the energy fraction deposited by inelastic processes ( $f_{elec}$ ) is higher (see Table 2). The fluence values were selected to simulate a deposited energy per unit volume comparable to the level after 1000 years in a monazite-brabantite matrix containing 10 oxide wt% minor actinides (Fig. 3). This corresponds to a nuclear damage range between 0.03 and about 7 dpa. The deposited energy per unit volume was calculated on the basis of simulations with SRIM 2003. The implantation was carried out at room temperature at the Orsay Nuclear and Mass Spectrometry Center [32], and the main characteristics are indicated in Table 3.

#### **Insert Table 3**

The ion energy values were selected to damage the material to depths compatible with the characterization tests used in this study (hardness, density, XRD, Raman spectroscopy) and to obtain a deposited nuclear or electronic energy per unit volume that was practically constant throughout the ion penetration depth. Multi-energy Au ion implantation at 1, 3.5 and 7 MeV was used to obtain a constant deposited nuclear energy to a depth of about 1.5  $\mu\text{m}$ ; under these conditions the deposited electronic energy was not constant. He ion

implantation (1.7 MeV) ensured a constant deposited electronic energy to a depth of 4 micrometers; in this case damage due to elastic interactions was very limited within the first few micrometers. At the highest He ion fluence levels the He concentration in the implantation peak reached significant values of about 2 at%.

### 2.3. Characterization

#### 2.3.1. Density

Density variations in the implanted materials were determined by measuring the irradiation-induced step height on the sample surface. A mask about 200  $\mu\text{m}$  thick with two slits was placed over the sample prior to irradiation. Ion implantation caused swelling or densification of the material, resulting in the appearance of steps at the slit positions. This measurement method is described in detail in references [33-34].

The step height was measured using a Wyko white-light optical interferometer. Given the ion implantation depth, density variations resulting from irradiation can then be determined:

$$\frac{\Delta\rho}{\rho} = \frac{\Delta V}{V} = \frac{100 \times Z}{P} \quad (3)$$

where  $Z$  is the step height in nanometers and  $P$  the ion implantation depth in nanometers. The depth corresponds to the x-coordinate of the point at which the nuclear or electronic energy loss ( $E_{nuc}$  or  $E_{elec}$ ) calculated by SRIM 2003 reaches 5% of the plateau value.

The volume expansion results obtained by this method are in good agreement with macroscopic swelling measurements of actinide-doped materials [33], substantiating the validity of this measurement method.

#### 2.3.2. Hardness measurement

The hardness of the monazite matrices was measured by Vickers microindentation on polished specimens implanted with Au and He ions, by applying a 1 to 5 g load for 15 seconds at a rate of 0.100 N/s. The microhardness was determined from the following relation:

$$Hv = \frac{2F \sin\left(\frac{136}{2}\right)}{d^2} \quad (4)$$

where  $Hv$  is the Vickers hardness (MPa),  $F$  the force applied (N), and  $d$  the mean length of the indentation diagonal (mm). For each characterization the hardness represents the mean of ten measurements. Based on results shown in Fig. 4, loads of less than 2 and 5 grams were used to measure microhardness variations on the samples implanted with gold and helium ions, respectively, so as to indent only the irradiated zone.

**Insert Figure 4**

### 2.3.3. XRD measurement

#### **Insert Figure 5**

Analyses were carried out using a Philips diffractometer with radiation  $\text{CuK}_\alpha$  radiation ( $\lambda = 1.5425 \text{ \AA}$ ) using a  $0.18^\circ$  parallel-plate collimator and a sealed proportional detector in the  $2\theta$  range from  $16$  to  $50^\circ$  in  $0.02^\circ$  steps and a counting time of  $110 \text{ s}$ .

The samples were analyzed at grazing incidence to characterize only the irradiation-damaged thickness on the sample surface. Successive measurements determined an incidence angle ( $2.3^\circ$ ) for which the analysis is characteristic of the irradiated layer (Fig. 5). The lattice parameters were calculated with TOPAS with hkl-phase refinement in full-profile matching mode.

### 2.3.4. Raman measurements

Raman microspectrometry spectra were obtained using a Labram Raman spectrometer and CCD detector coupled with an Olympus optical microscope. The sample was illuminated by a YAG laser beam at a wavelength of  $532 \text{ nm}$ . A  $100\times$  objective and  $1800 \text{ lines/mm}$  grating were used. The spectra were recorded between  $70 \text{ cm}^{-1}$  and  $1470 \text{ cm}^{-1}$  with a spectral resolution of  $2 \text{ cm}^{-1}$ . The structural data from the outer micrometers at the surface of the irradiated samples were determined by combining confocal Raman microscopy (with an axial resolution of  $2 \text{ }\mu\text{m}$ ) with a motorized z-stage to obtain relative band profile variations.

## **3. Results**

### 3.1. Ion implantation depth

The ion implantation depth estimated from SRIM 2003 simulations was about  $1.5 \text{ }\mu\text{m}$  in the case of irradiation with gold ions. The estimated value is in close agreement with the value measured by transmission electron microscopy on thin sections obtained by the Focused Ion Beam at the GFZ-Potsdam [35] technique on a  $\text{La}_{0.73}\text{Ce}_{0.27}\text{PO}_4$  sample irradiated at the highest fluence (Fig. 6).

#### **Insert Figure 6**

### 3.2. Swelling measurements

Irradiation by Au ions resulted in significant swelling of both ceramic matrices. The swelling saturated at about  $8\%$  for an irradiation fluence exceeding  $10^{14} \text{ at/cm}^2$ . Helium implantation caused slight swelling (about  $0.8\%$ ) of the  $\text{LaPO}_4$  matrix (Fig. 7).

#### **Insert Figure 7**

### 3.3. Hardness measurements

Figure 10 summarizes the hardness values measured on the materials irradiated by gold and helium. The hardness of the materials irradiated by gold ions diminished, stabilizing at about 3000 MPa for a fluence exceeding  $10^{14}$  at/cm<sup>2</sup> (i.e.  $10^{21}$  keV/cm<sup>3</sup>). The hardness variation for both monazite matrices was very similar. At the highest fluence  $F_6$  ( $2.3 \times 10^{15}$  at/cm<sup>2</sup>) a hardness reduction of about 59% compared with the initial value was observed for both monazite matrices. Figure 10 shows that the hardness of the two matrices irradiated by helium ions did not vary beyond the measurement uncertainty range.

### 3.4. XRD measurements

The diffraction peaks of monazites LaPO<sub>4</sub> gradually disappeared as the gold ion fluence increased. Above the fluence  $F_4$  ( $9.3 \times 10^{13}$  at/cm<sup>2</sup>), the structure diffraction peaks broadened and some reflections disappeared. Amorphization was practically complete at fluence  $F_5$  ( $7.2 \times 10^{14}$  at/cm<sup>2</sup>). Au ion implantation thus destroyed the long-range crystalline order, whereas irradiation with helium ions had no effect. Table 4 indicates the unit cell volume versus the fluence, and the amorphous fraction for monazites irradiated with gold ions. Broadening of the diffraction peaks above fluence  $F_1$  ( $9.6 \times 10^{12}$  at/cm<sup>2</sup>) made it impossible to determine the unit cell volume.

#### **Insert Table 4**

### 3.5. Raman measurements

Raman microspectrometry analyses were performed on pristine monazite and on gold-irradiated monazite. The signature of the four internal vibration modes of the PO<sub>4</sub><sup>3-</sup> phosphate group ( $\nu_s$  between 950-1000 cm<sup>-1</sup>;  $\nu_{as}$  between 1020-1150 cm<sup>-1</sup>;  $\delta_s$  between 350-450 cm<sup>-1</sup>;  $\delta_{as}$  between 560-630 cm<sup>-1</sup> [36]) was effective regardless of the irradiation fluence (Fig. 8).

#### **Insert Figure 8**

According to Nasdala [37-38] and Seydoux-Guillaume [6] the loss of short-range order in the zircon compound (ZrSiO<sub>4</sub>) is apparent in the Raman spectra in the form of broader bands shifted toward lower wave numbers. In our study, despite slight broadening of a few bands attributable to the measurement statistics ( $\nu_s$  vibration), the peaks can be considered to remain narrow. The phosphate tetrahedra therefore do not appear to be affected by irradiation. The existence of these bands even at the highest fluence values when the crystalline order has disappeared shows that the material is not completely damaged. Irradiation with gold ions thus results in amorphization of the crystal lattice (long-range order) but does not locally destroy the PO<sub>4</sub><sup>3-</sup> polyhedra.



## 4. Discussion

### 4.1. Effect of the type of deposited energy on the behavior of monazite

#### 4.1.1. Deposited electronic energy

As noted above, irradiation by helium ions is intended to simulate the impact of electronic interactions. No change in the structure of helium-implanted monazites was observed over the full experimental fluence range. The X-ray diffraction diagrams measured on monazites implanted with helium ions at fluence  $F'_5$  ( $5.43 \times 10^{16}$  at/cm<sup>2</sup>) were comparable to that of unimplanted monazite. Moreover, no significant change was observed in the hardness of the test samples. No monazite swelling was observed for deposited energy values below  $7.5 \times 10^{22}$  keV<sub>elec</sub>/cm<sup>3</sup>. Slight swelling, however, less than 0.8%, was observed for the highest fluence corresponding to a deposited electronic energy of  $2.8 \times 10^{23}$  keV<sub>elec</sub>/cm<sup>3</sup>. This volume expansion could perhaps be related to helium accumulation, which locally exceeded 2 at% (Table 3).

All these results show that energy losses through electronic interactions resulting from helium implantation do not affect the macroscopic, mechanical, and structural properties of monazite matrices within the experimental fluence range.

#### 4.1.2. Deposited nuclear energy

As noted above, irradiation by gold ions is intended to simulate the impact of nuclear interactions. Gold ion implantation resulted in swelling of the monazite matrices by up to 8.1% at the highest fluence (Fig. 9). Moreover, X-ray diffraction diagrams showed amorphization of the monazite matrices under ion irradiation as the fluence increased.

The amorphous fraction and macroscopic swelling (Fig. 9) varied in similar fashion with the deposited nuclear energy. For a deposited nuclear energy level of  $10^{21}$  keV/cm<sup>3</sup>, the amorphous monazite fraction exceeded 90% and the structure volume expansion stabilized. The correlation between these two phenomena indicates that the ballistic processes which generate point defects, and thus amorphization, in monazite are responsible for these changes. This finding suggests another interpretation for the 0.8% volume expansion observed in monazite irradiated by ions He at the highest fluence (Fig. 7), which could be attributable to energy losses through nuclear interactions, which are no longer negligible near the end of the helium particle range.

### Insert Figure 9

Finally, the hardness of monazite diminishes by about 59% with the deposited nuclear energy, and once again stabilizes for a deposited nuclear energy exceeding  $5 \times 10^{20}$  keV<sub>nucl</sub>/cm<sup>3</sup> (Fig. 10). The evolution of this property also appears to be related to the creation of point defects in the structure.

## Insert Figure 10

The results obtained show that only nuclear effects result in major modifications of the macroscopic, mechanical, and structural properties of monazite matrices at the tested fluence levels: the deposited nuclear energy ( $10^{21}$  keV/cm<sup>3</sup>) corresponding to monazite amorphization and stabilization of these properties is the same, and no changes in volume or hardness were observed versus the deposited electronic energy.

### 4.2. Irradiation stability of the phosphate group?

The results of this study showed that the deposited nuclear energy is responsible for amorphization of the monazite compound, but that this parameter does not affect the stability of the phosphate group. The same conclusion was reached by Tamain [41] on Thorium phosphate diphosphate compound  $\text{Th}_4(\text{PO}_4)_4\text{P}_2\text{O}_7$  with phosphate groups. She showed that irradiation by 4 MeV gold ions resulted in amorphization of this structure, whereas—as with monazite—irradiation by helium ions did not lead to structural changes. The variation in the amorphous fraction calculated from diffraction diagrams was comparable to that observed for monazite (Fig. 11).

## Insert Figure 11

Only nuclear effects modify the structural properties of  $\text{Th}_4(\text{PO}_4)_4\text{P}_2\text{O}_7$  compounds at the tested fluence values. Irradiation of the same compounds with 840 MeV Kr ions led to amorphization of the material, but did not damage the P-O chemical bonds [41]. A similar result was also reported for actinide-doped monazites. The Raman spectra of  $^{243}\text{AmPO}_4$ ,  $^{248}\text{CmPO}_4$ ,  $^{249}\text{CfPO}_4$ ,  $^{249}\text{BkPO}_4$  and  $^{253}\text{EsPO}_4$  show well defined bands indicating conservation of the phosphate group [42] whereas  $^{241}\text{AmPO}_4$  is amorphous for doses of about  $8.3 \times 10^{17}$  a/g [16].

Work with  $M_{10}(\text{XO}_4)_6\text{Y}_2$  phosphosilicates, where  $M = \text{Ca}^{2+}, \text{Sr}^{2+}, \text{Pb}^{2+}$  etc.,  $\text{XO}_4 = \text{PO}_4^{3-}, \text{VO}_4^{3-}, \text{SiO}_4^{4-}$  etc., and  $Y = \text{F}, \text{OH}, \text{Cl}$  etc., showed greater irradiation sensitivity at higher  $\text{SiO}_4/\text{PO}_4$  ratios [43]. Studies of natural apatite also showed that minerals with high silicate content are more sensitive to irradiation [44]. Soulet attributes this result to the fact that the phosphate group in the structure favors annealing of the matrix by  $\alpha$  irradiation [43]. Meldrum [39] also reported that  $M\text{PO}_4$  phosphate compounds are characterized by lower annealing temperatures and activation energies than  $M\text{SiO}_4$  silicate compounds; he attributed this difference to P-O bonds, much stronger and shorter than Si-O bonds [23].

## 5. Conclusion

Monazite matrices were irradiated with gold and helium ions to assess the relative effects of the resulting electronic and nuclear interactions. Only nuclear interactions led to major modifications of the matrix properties within the tested fluence range. A damage dose of 6.7 dpa resulted in 8.1% volume expansion, a 59% hardness

reduction, and amorphization of the test matrices, although Raman spectroscopy analysis showed that the phosphate groups were not affected. There appear to be two material damage levels, as observed for the phosphate compound  $\text{Th}_4(\text{PO}_4)_4\text{P}_2\text{O}_7$  irradiated by high-energy ions. The large-scale crystalline order is destroyed, while locally the chemical groups remain intact.

Although monazite become amorphous after irradiation, natural analogs and  $(\text{La}, \text{An})\text{PO}_4$  compounds remain crystallized. Further studies will be necessary to assess the behavior of monazite matrices under self-irradiation with lower dose rate.  $^{238}\text{Pu}$ -doped monazite-brabantite matrices ( $\text{La}_{1-x-2y}^{238}\text{Pu}_x^{+III}\text{Ca}_y\text{Th}_y^{+IV}\text{PO}_4$ ) are currently being investigated in the Atalante DHA laboratory to monitor the effects of alpha decay damage on the physical properties of the matrices.

## References

- [1] L.A. Boatner, M.M. Abraham, B.C. Sales, *Inorg. Chim. Acta* 94 (1984) 146-148.
- [2] C.M. Gramaccioli, T.U. Segalstad, *Am. Miner.* 63 (1978) 757-761.
- [3] L.A. Boatner, B.C. Sales, Monazite, Radioactive waste forms for the future, in: Lutze W. and Ewing R. C. (Eds.), *Radioactive waste forms for the future*, pp. 495-564, 1988.
- [4] J-M. Montel, S. Foret, M. Veschambre, C. Nicollet, A. Provost, *Chem. Geol.*, 131 (1996) 37-53.
- [5] E.H. Oelkers, F. Poitrasson, *Chem. Geol.*, 19 (2002) 73-87.
- [6] A. M. Seydoux-Guillaume, R. Wirth, L. Nasdala, M. Gottschalk, J-M. Montel, W. Heinrich, *Phys. Chem. Miner.*, 29 (2002) 240-253.
- [7] A. M. Seydoux-Guillaume, R. Wirth, A. Deutsch, U. Schärer, *Geoch. Cosmochim. Acta*, 68 (2004) 2517-2527.
- [8] A. M. Seydoux-Guillaume, R. Wirth, J. Ingrin, *Eur. J. Miner.*, 19 (2007) 7-14.
- [9] A. Meldrum, L.A. Boatner, R.C. Ewing, *Miner. Mag*, 64 (2000) 183-192.
- [10] C.W. Bjorklund, *J. Am. Chem. Soc.*, 79 (1958) 6347-6350.
- [11] C.E. Bamberger, R.G. Haire, H.E. Hellwege, G.M. Begun, *J. Less-Common Met.*, 97 (1984) 349-356.
- [12] A.S. Aloy, E.N. Kovarskaya, T.I. Koltsova, S.E. Samoylov, S.I. Rovnyi, G.M. Medvedev, L.J. Jardine, Radioactive Waste management and Environmental Remediation, in *Proceeding of the 8<sup>th</sup> International Conference on Environmental Management*, Bruges, Belgium, pp. 1833-1836, 2001.
- [13] C. Keller, K.H. Walter, *J. Inorg. Nucl. Chem.*, 27 (1965) 1253-1260.
- [14] V.F. Weigel, H. Haug, *Radiochim. Acta*, 4 (1965) 227-228.
- [15] K.L. Kelly, G.W. Beall, J.P. Young, L.A. Boatner, in *Scientific Basis for Nuclear Waste Management*, 3, (Eds. Plenum), pp.189-195, 1981.
- [16] D. Bregiroux, R. Belin, P. Valenza, F. Audubert, D. Bernache-Assollant, *J. Nucl. Mater.*, 366 (2007) 52-57.

- [17] A. Tabuteau, M. Pagès, J. Livet, C. Musikas, *J. Mater. Sci. Let.*, 7 (1988) 1315-1317.
- [18] Y. Dusausoy, N.E. Ghermani, R. Podor, M. Cuney, *Eur. J. Miner.*, 8 (1996) 667-673.
- [19] R. Podor, M. Cuney, *Am. Miner.*, 82 (1997) 765-771.
- [20] X. Deschanel, V. Picot, B. Glorieux, F. Jorion, S. Peugeot, D. Roudil, C. Jegou, V. Broudic, J-N. Cachia, T. Advocat, C. Den Auwer, C. Fillet, J-P. Coutures, C. Hennig, A. Scheinost, *J. Nucl. Mater.*, 352 (2006) 233-240.
- [21] B.E. Burakov, M.A. Yagovkina, V.M. Garbuzov, A.A. Kitsay, V.A. Zirlin, in *Scientific Basis for Nuclear Waste Management XXVIII*, J.M. Hanchar (Eds.), San Fransico, California, Vol. 824, pp. 219-224, 2004.
- [22] D. Bregiroux, PhD thesis, Université de Limoges 16 Novembre 2005.
- [23] A. Meldrum, L.A. Boatner, L.M. Wang, R.C. Ewing, *Nucl. Instr. Meth. Phys. Res. B*, 127/128 (1997) 160-165.
- [24] A. Meldrum, L.A. Boatner, R.C. Ewing, *Am. Phys. Soc. B*, 56 (1997) 13805-13814.
- [25] F.G. Karioris, K. Appaji Gowda, L. Cartz, *Rad. Eff. Lett.*, 58 (1981) 1-3.
- [26] A. Meldrum, L.A. Boatner, R.C. Ewing, *J. Mater. Res.*, 12 (1997) 1816-1827.
- [27] J-M. Montel, B. Glorieux, A.M. Seydoux-Guillaume, R. Wirth, *J. Phys. Chem. Solids*, 67 (2006) 2489-2500.
- [28] Y. Ni, J.M. Hughes, A.N. Mariano, *Am. Miner.*, 80 (1995) 21-26.
- [29] G.H. Kinchin, R.S. Pease, *Reports Prog. Phys.*, 18 (1955) 1-51.
- [30] W.J. Weber, R.C. Ewing, C.R.A. Catlow, T.D. de la Rubia, L.W. Hobbs, C. Kinoshita, H.J. Matzke, A.T. Motta, M. Nastasi, E.K.H. Salje, E.R. Vance, S.J. Zinkle, *J. Mater. Res.*, 13 (1998) 1434-1484.
- [31] J.F. Ziegler, P. Biersack, U. Littmark, *The stopping and ranges of ions in matter*, Vol. 1, Eds. Pergamon Press, New York, 1985.
- [32] E. Cottureau, J. Camplan, J. Chaumont, J. Meunier, H. Bernas, *Nucl. Instr. Meth. Phys. Res. B*, 45 (1990) 293-295.
- [33] S. Peugeot, J-L. Loubet, S. Pavan, S. Henry, C. Peaucelle, V. Picot, X. Deschanel, P. Nivet, in *Proceedings Congress Matériaux, 2006, Dijon, France*.
- [34] V. Picot, X. Deschanel, S. Peugeot, B. Glorieux, C. Fillet, G. Blondiaux, in *Proceedings Congress Matériaux, 2006, Dijon, France*.
- [35] R. Wirth, *Eur. J. Mineral.*, 16 (2004) 863-877.
- [36] G.M. Begun, G.W. Beall, L.A. Boatner, W.J. Gregor, *J. Raman Spectros.*, 11 (1981) 273-278.
- [37] L. Nasdala, D. Wolf, G. Irmer, *Eur. J. Miner.*, 7 (1995) 471-478.
- [38] L. Nasdala, C.L. Lengauer, J.M. Hanchar, A. Kronz, R. Wirth, P. Blanc, A.K. Kennedy, A.M. Seydoux-Guillaume, *Chem. Geol.*, 191 (2002) 121-140.
- [39] A. Meldrum, L.W. Wang, R.C. Ewing, *Nuc. Instr. Meth. Phys. Res. B*, 116 (1996) 220-224.
- [40] A. Meldrum, L.A. Boatner, W.J. Weber, R.C. Ewing, *Geoch. Cosmochim. Acta*, 62 (1998) 2509-2520.

- [41] C. Tamain, F. Garrido, L. Thome, N. Dacheux, A. Ozgumus, A. Benyagoub, *J. Nucl. Mater.*, 357 (2006) 206-212.
- [42] D.E. Hobart, G.M. Begun, R.G. Haire, H.E. Hellwege, *J. Raman Spectros.*, 14 (1983) 59-62.
- [43] S. Soulet, J. Carpena, J. Chaumont, O. Kaitasov, M.O. Ruault, J.C. Krupa, *Nuc. Instr. Meth. Phys. Res. B*, 184 (2001) 383-390.
- [44] J. Carpena, J.R. Kienast, K. Ouzegane, C. Jehanno, *Geol. Soc. Am. Bull*, 100 (1998) 1237-1243.

Table 1. Properties of starting materials

Characteristics	LaPO <sub>4</sub>	La <sub>0.73</sub> Ce <sub>0.27</sub> PO <sub>4</sub>	LaPO <sub>4</sub> from ref. [19]	La <sub>0.73</sub> Ce <sub>0.27</sub> PO <sub>4</sub> from ref. [19, 28]
Geometrical density (g·cm <sup>-3</sup> )	4.86 ± 0.04	4.73 ± 0.09	-	-
Relative density (%)	95 ± 1	92.5 ± 2	-	-
Crystal parameters				
a (Å)	6.8396(4)	6.8253(8)	6.837	6.824
b (Å)	7.0733(4)	7.0606(8)	7.077	7.061
c (Å)	6.5112(4)	6.4953(5)	6.510	6.498
β (°)	103.288(3)	103.318(5)	103.24	103.29
V (Å <sup>3</sup> )	306.57(2)	304.59(3)	306.50	304.68

Table 2. Fraction of initial energy transferred by ionization and electronic excitation ( $f_{elec}$ ) and by ballistic processes ( $f_{nucl}$ ) in actinide-doped monazite irradiated externally, based on SRIM 2003 simulations [31].

	La <sub>0.87</sub> Cm <sub>0.006</sub> Am <sub>0.044</sub> Ca <sub>0.04</sub> Np <sub>0.04</sub> PO <sub>4</sub>		Externally irradiated LaPO <sub>4</sub>	
	Recoil nucleus	$\alpha$ particle	Au	He
	(100 keV)	(5 MeV)	(1, 3.5 & 7 MeV)	(1.7 MeV)
$f_{elec}$ (%)	39	99.8	74	99.5
$f_{nucl}$ (%)	61	0.2	26	0.5

Table 3. External irradiation characteristics

He irradiation (1.7 MeV)						
	F <sub>1</sub>	F <sub>2</sub>	F <sub>3</sub>	F <sub>4</sub>	F <sub>5</sub>	
Fluence (at/cm <sup>2</sup> )	1.09 × 10 <sup>15</sup>	2.88 × 10 <sup>15</sup>	6.30 × 10 <sup>15</sup>	1.67 × 10 <sup>16</sup>	5.43 × 10 <sup>16</sup>	
Maximum implanted concentration (ppm)	464	1227	2684	7116	23137	
$E_{nucl} \times 10^{20}$ (keV/cm <sup>3</sup> )*	0.11	0.29	0.63	1.7	5.4	
$E_{elec} \times 10^{20}$ (keV/cm <sup>3</sup> )	49	130	280	750	2400	
Au irradiation (1, 3.5 & 7 MeV)						
	F <sub>1</sub>	F <sub>2</sub>	F <sub>3</sub>	F <sub>4</sub>	F <sub>5</sub>	F <sub>6</sub>
Fluence (at/cm <sup>2</sup> )	9.6 × 10 <sup>12</sup>	1.73 × 10 <sup>13</sup>	3.8 × 10 <sup>13</sup>	9.6 × 10 <sup>13</sup>	7.2 × 10 <sup>14</sup>	2.3 × 10 <sup>15</sup>
Maximum implanted concentration (ppm)	2	3	6	16	115	376
$E_{nucl} \times 10^{20}$ (keV/cm <sup>3</sup> )	1	1.8	4	11	79	250
$E_{elec} \times 10^{20}$ (keV/cm <sup>3</sup> )	2.8	5.1	11	29	220	700
dpa	0.03	0.05	0.11	0.28	2.11	6.7

\* $E_{nucl}$  was calculated for a mean nuclear damage depth of 2.7 μm as determined by Vickers microindentation.



Table 4. Mesh cell volume versus fluence and normalized area of diffraction peak (120) of LaPO<sub>4</sub> monazite compounds irradiated by gold ions

Fluence (at/cm <sup>2</sup> )	0	9.6 x 10 <sup>12</sup>	3.8 x 10 <sup>13</sup>	9.6 x 10 <sup>13</sup>	7.2 x 10 <sup>14</sup>	2.3 x 10 <sup>15</sup>
$V (\text{\AA}^3)$	304.2 (5)	304.4 (2)	-	-	-	-
$I_{(120)}$ cps	1726	1360	180	171	136	69
$f_{amorph} = (I_{(120)} - I_{(120)}) / I_{(120)}$	0	0.21	0.895	0.9	0.92	0.96

## Liste of Figures

Figure 1. SEM image of  $\text{LaPO}_4$  ceramic sintered for 4 h at  $1450^\circ\text{C}$ .

Figure 2 : SEM image of  $\text{La}_{0.73}\text{Ce}_{0.27}\text{PO}_4$  ceramic sintered for 4 h at  $1450^\circ\text{C}$ .

Figure 3. Integrated dose and number of dpa [29] versus time after disposal of a monazite-brabantite matrix,  $\text{La}_{0.87}\text{Ce}_{0.006}\text{Am}_{0.044}\text{Ca}_{0.04}\text{Np}_{0.04}\text{PO}_4$ , corresponding to 10 oxide wt% minor actinides in the proportions found in the output flows from reprocessing of the benchmark spent fuel [20]. The shaded zone corresponds to the range simulated by external irradiation.

Figure 4. Vickers hardness variation versus applied load on a pristine monazite  $\text{LaPO}_4$  implanted with Au ions with a fluence of  $2.3 \times 10^{15}$  at/cm<sup>2</sup>.

Figure 5. (120) reflection versus incidence angle of monazite  $\text{LaPO}_4$  irradiated by Au ions at highest fluence.

Figure 6. TEM-BF (Bright Field) image showing the thickness of the irradiated zone in a monazite  $\text{La}_{0.73}\text{Ce}_{0.27}\text{PO}_4$  sample irradiated by gold ions at a fluence of  $2.3 \times 10^{15}$  cm<sup>-2</sup>. The amorphous zone recrystallized under electron beam.

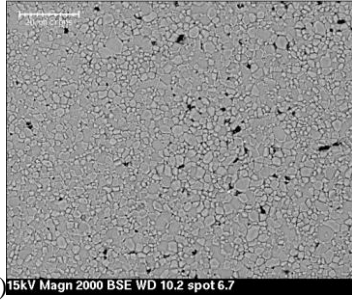
Figure 7. Volume expansion versus fluence in materials implanted with Au and He ions.

Figure 8. Raman microspectrometry spectra of pristine and gold-irradiated monazites.

Figure 9. Amorphous fraction and macroscopic swelling versus  $E_{nucl}$  for  $\text{LaPO}_4$  ceramic.

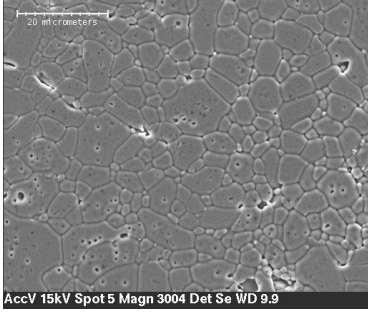
Figure 10. Hardness variations of materials implanted with Au and He ions versus  $E_{nucl}$ .

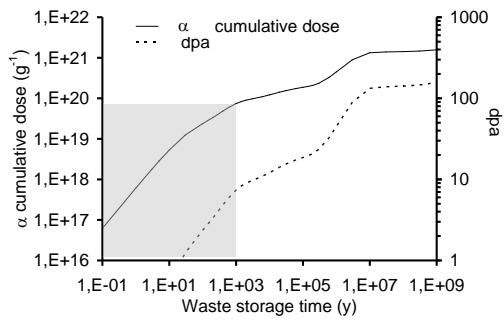
Figure 11. Comparison of amorphous fraction versus  $E_{nucl}$ . in  $\text{LaPO}_4$  and (TPD)  $\text{Th}_4(\text{PO}_4)_4\text{P}_2\text{O}_7$  ceramics.



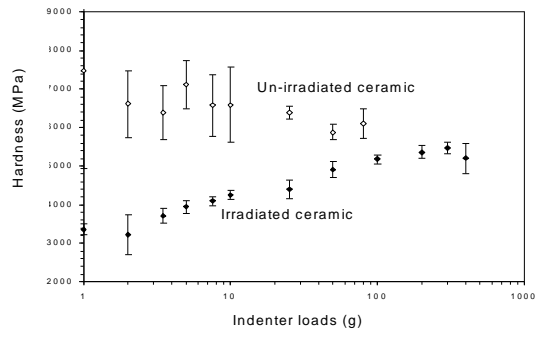
(1)

15kV Magn 2000 BSE WD 10.2 spot 6.7

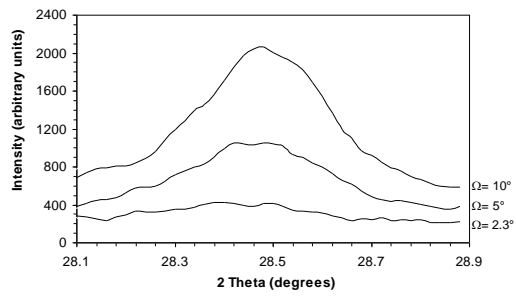




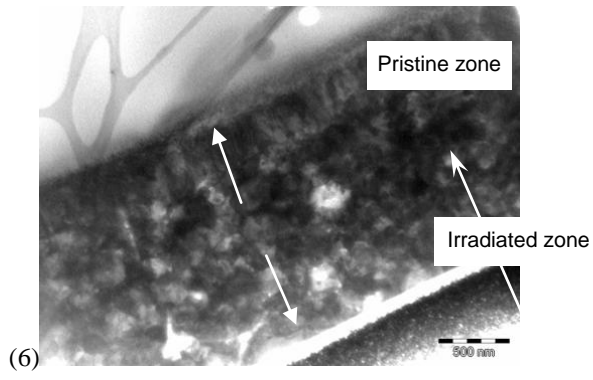
(3)



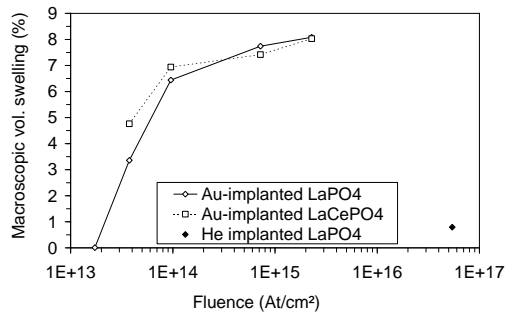
(4)



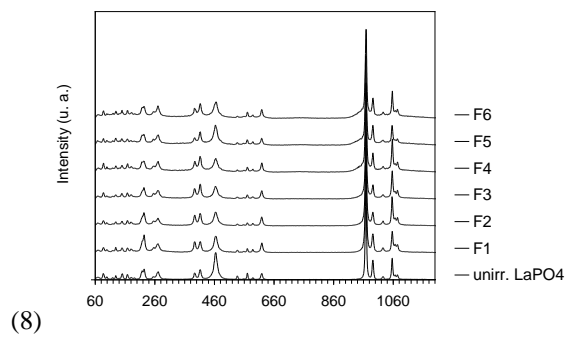
(5)

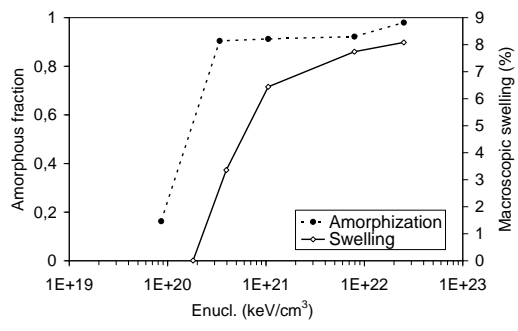




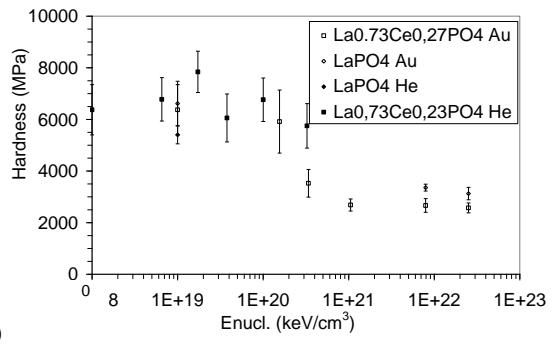


(7)

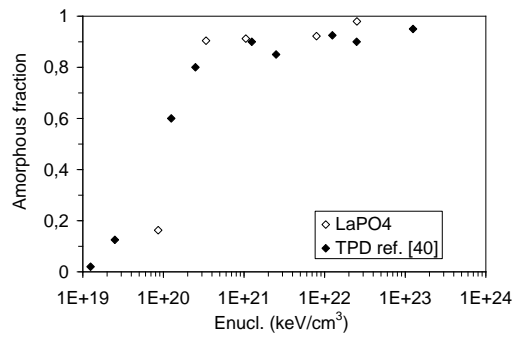




(9)



(10)



(11)